Journal of Structural Geology 33 (2011) 1501–1508

Contents lists available at ScienceDirect

Journal of Structural Geology

journal homepage: www.elsevier.com/locate/jsg

The neutral lines in buckle folds

Marcel Frehner*,[1]

Department for Geodynamics and Sedimentology, University of Vienna, Austria

ARTICLE INFO

Article history:
Received 8 February 2011
Received in revised form
20 June 2011
Accepted 18 July 2011
Available online 27 July 2011

Keywords:
Neutral line
Neutral surface
Buckle folds
Folding
Tangential longitudinal strain
Finite element method

ABSTRACT

The neutral line in a buckle fold, dividing areas of outer-arc extension from areas of inner-arc shortening, is a fundamental concept in structural geology. In the past, folds have been constructed kinematically from a given neutral line geometry using the tangential longitudinal strain pattern. In this study, a mechanical finite element model is used to numerically buckle single-layer folds with Newtonian and power-law viscous rheology. Two neutral lines can be distinguished, the incremental neutral line (zero layer-parallel strain rate) and the finite neutral line (zero finite layer-parallel strain). The former develops first and migrates through the layer from the outer towards the inner arc ahead of the latter. Both neutral lines are discontinuous along the fold and terminate either at the bottom or top interface of the layer. For decreasing viscosity ratio between layer and matrix and for decreasing initial amplitude, the neutral lines develop later during folding and, for some cases, no neutral line develops. The dynamical behaviour of the neutral lines is similar for Newtonian and power-law viscous rheology if the viscosity ratio is large, but substantially different for small viscosity ratios. The results are discussed in light of fold-related structures, such as outer-arc-extension structures and inner-arc-shortening structures.

1. Introduction

In structural geology, the concept of the neutral line is fundamental for characterizing folds. Descriptions and sketches can be found in almost every classical and modern structural geology textbook (e.g., Ramsay, 1967; Ramsay and Huber, 1987; Price and Cosgrove, 1990; Twiss and Moores, 2007; Fossen, 2010). Usually, the neutral line is described as the line in the fold profile, on which the principal strains are zero (Ramsay, 1967). In other words, the neutral line separates areas of layer-parallel extension in the outer arc of the fold (referred to as outer-arc extension) from areas of layer-parallel shortening in the inner arc (referred to as inner-arc shortening). Indeed, in natural folds so-called outer-arc-extension structures and inner-arc-shortening structures can be observed. For example, Fig. 1 shows a folded limestone multilayer sequence exhibiting a thrust in the innermost layer, which reflects the shortening in the inner arc. A common outer-arc-extension structure is a set of layer-perpendicular extensional fractures, an example of which is shown in Fig. 2 in a quartzwacke-layer. The layer-parallel extension in the outer arc is evident from the opening direction of the fractures. Other outer-arc-extension structures and inner-arc-shortening structures are, for example, stylolites or the development of an enhanced foliation (Ramsay and Huber, 1987). For a recent extensive review on the mechanical and kinematical understanding and interpretation of folds, see Hudleston and Treagus (2010).

The neutral line has been used for the kinematical analysis and construction of folds by assuming an idealized strain pattern called tangential longitudinal strain (TLS; Ramsay, 1967; Ramsay and Huber, 1987; Bobillo-Ares et al., 2000, 2004; Bastida et al., 2003, 2005; Bobillo-Ares et al., 2006). Different versions of TLS can be found in the literature, all with slightly different sets of assumptions. One fundamental assumption common to all versions of TLS is a neutral line that is continuous along the fold (i.e., from the axial plane trace of an antiform to the axial plane trace of the adjacent synform). This assumption is an implicit part of the TLS strain pattern, because the fold is constructed from a given neutral line geometry. However, Gairola (1978) and Currie et al. (1962) showed that the neutral line, at least in experimentally folded layers, is not continuous along the fold. For a more complete kinematical fold analysis, other strain patterns, such as flexural flow or homogeneous pure-shear strain, are usually applied on top of TLS (Bastida et al., 2003; Bobillo-Ares et al., 2004). TLS is also referred to as orthogonal flexure (Twiss and Moores, 2007) and neutral line folding (Lisle et al., 2009) and has been applied, for example, to the kinematical analysis of symmetrical folds (Hudleston and Holst, 1984; Toimil and Fernandez, 2007), asymmetrical folds (Aller et al., 2010) and chevron folds (Bastida et al., 2007).

* Tel.: +41 44 632 5468; fax: +41 44 632 1030.
E-mail address: marcel.frehner@erdw.ethz.ch.
[1] Present address: Geological Institute, ETH Zurich, Sonneggstrasse 5, 8092 Zurich, Switzerland.

0191-8141/$ – see front matter © 2011 Elsevier Ltd. All rights reserved.
doi:10.1016/j.jsg.2011.07.005

Fig. 1. Folded Triassic limestone–marl multilayer sequence near Bad Eisenkappel, Austria [Lat. 46.450857°/Lon. 14.477277°]. Shortening in the inner arc of the multilayer fold is evident from an inner-arc-shortening structure, i.e., a brittle thrust of approx. 20 cm offset. Picture courtesy of Lea Hilty.

In contrast to kinematical fold analysis methods, mechanical models take the mechanical and rheological behaviour of the folded rocks into account. Structures inside the folding layer develop self-consistently according to the applied continuum mechanics equations. Therefore, mechanical models of folding do not a priori assume a neutral line geometry, but the neutral line results from the modelled buckling process. Mechanical models, in particular numerical finite element (FE) models, have been used to study the neutral line in buckle folds. Early FE-studies (e.g., Dieterich, 1969; Dieterich and Carter, 1969; Shimamoto and Hara, 1976) visualized the orientation of the principal stresses or the principal strains, from which a separation between outer-arc extension and inner-arc shortening is evident. Hudleston and Lan (1993) and Hudleston and Lan (1995) calculated the aspect ratio of the finite strain ellipses on the axial plane trace to quantify the outer-arc extension and the inner-arc shortening. In addition, Lan and Hudleston (1995) defined two neutral lines according to Ramsay (1967), i.e., the finite neutral line (FNL) and the incremental neutral line (INL), and they found that on the axial plane trace both neutral lines migrate through the layer from the outer towards the inner arc with increasing shortening. However, the geometry of the neutral lines away from the axial plane trace has only been sketched schematically (Hudleston and Lan, 1995; Lan and Hudleston, 1995; also Twiss and Moores, 2007; Hudleston and Treagus, 2010).

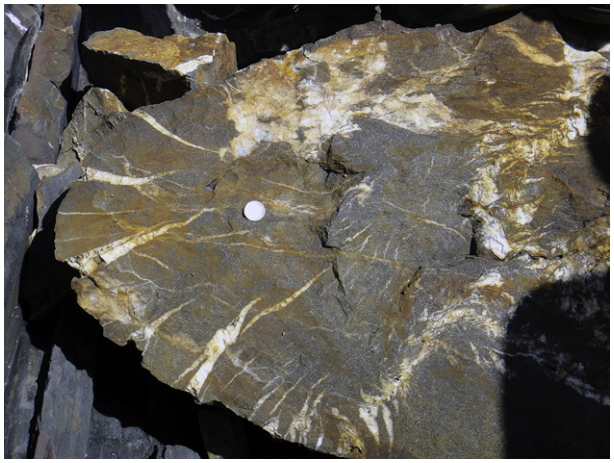

Fig. 2. Folded Carboniferous quartzwacke-layer (Lechmann et al., 2010) near Almograve, Portugal [Lat. 37.658761/Lon. −8.802215]. Extension in the outer arc of the fold is evident from outer-arc-extension structures, i.e., quartz-filled extensional fractures perpendicular to the folded layer.

This study applies the FE method to simulate the dynamical behaviour of the neutral lines in a two-dimensional mechanically calculated buckle fold. The paper starts with a short introduction to the used model setup and it is explained in detail how the INL and the FNL are calculated from the numerical simulations. Both neutral lines are visualized and quantitatively described for single-layer buckle folds with either Newtonian or power-law viscous rheology. The dynamical behaviour of the two neutral lines is discussed in light of interpreting fold-related structures, such as outer-arc-extension structures and inner-arc-shortening structures.

2. Model setup

Because for this study, folds are assumed to be cylindrical (i.e., no geometry change along the fold axis), it is sufficient to use a model that describes the deformation in two dimensions (2D) with a plane-strain formulation. The rheological behaviour of both the folding layer and the surrounding matrix is incompressible power-law viscous, given by the constitutive equations in the x_1–x_2-coordinate system,

$$\sigma_{ij} = -\delta_{ij}\left(p + \frac{2}{3}\eta_{\mathrm{eff}}\frac{\partial v_k}{\partial x_k}\right) + \eta_{\mathrm{eff}}\left(\frac{\partial v_i}{\partial x_j} + \frac{\partial v_j}{\partial x_i}\right) \tag{1}$$

$$\eta_{\mathrm{eff}} = \eta_0 \dot{\varepsilon}_{\mathrm{II}}^{(1/(n-1))} \tag{2}$$

$$\dot{\varepsilon}_{\mathrm{II}} = \frac{1}{2}\sqrt{\left(\frac{\partial v_1}{\partial x_1} - \frac{\partial v_2}{\partial x_2}\right)^2 + \left(\frac{\partial v_1}{\partial x_2} + \frac{\partial v_2}{\partial x_1}\right)^2} \tag{3}$$

In Eqs. (1)–(3) σ_{ij} are the three independent components of the symmetrical 2D stress tensor, p is the pressure (i.e., negative mean normal stress), v_i are the two components of the 2D velocity vector, η_{eff} is the effective dynamic viscosity, η_0 is the reference dynamic viscosity, i.e., the dynamic viscosity for a given reference strain rate (1 in the present study), $\dot{\varepsilon}_{\mathrm{II}}$ is the second strain rate invariant, and n is the power-law exponent. For $n = 1$ the material is linear viscous (Newtonian). Index k in Eq. (1) implies a summation from 1 to 2. Gravity in the Stokes equations is set to zero, because it is assumed that gravitational effects are negligible for the folds considered in this study.

The 2D numerical model domain (Fig. 3) is bounded by an initially rectangular box of width $\lambda_0/2$. The boundary conditions are: no traction and no boundary-perpendicular velocity (immobile free slip wall) at the lower and left boundaries; no traction (free surface) at the top boundary; and no traction with a prescribed horizontal velocity (moving free slip wall) at the right boundary. The prescribed horizontal velocity is modified at every time step to enforce a constant background shortening strain rate, $\dot{\varepsilon}_{\mathrm{ext}}$. In the middle of the modelling box a horizontal layer of initial thickness h_0 has a higher reference viscosity than the surrounding matrix ($\eta_{0,\mathrm{L}} > \eta_{0,\mathrm{M}}$; Table 1) and perfectly welded interfaces. To allow the folding instability to develop, both interfaces have the same sinusoidal initial geometry with a small amplitude, $A_0/h_0 << 1$ (Table 1). In this study only upright symmetrical folds with dominant initial wavelength under horizontal shortening are considered. In such folds the vertical axial plane represents a traction-free surface. Due to this symmetry reason only half a wavelength is simulated (from the axial plane trace of an antiform to the axial plane trace of the

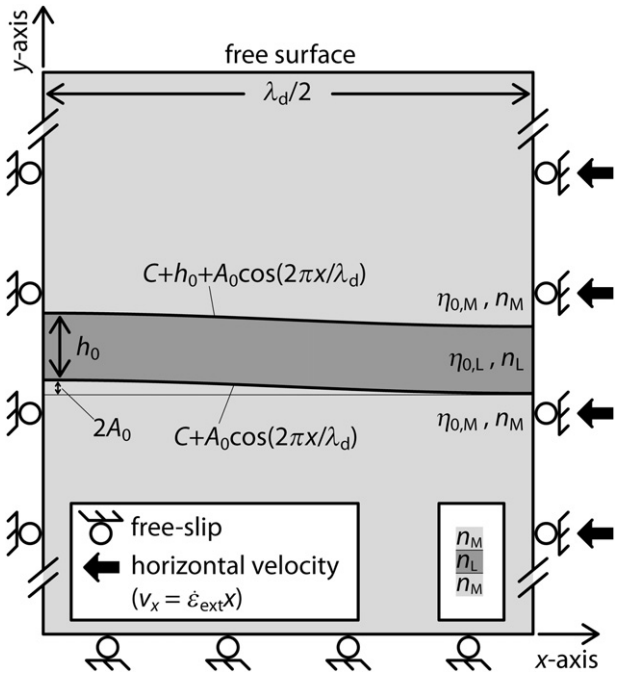

Fig. 3. Sketch (not to scale) showing the model domain, the initial conditions, and the boundary conditions for the numerical simulations. For more details see Table 1. In the lower-right corner the symbol used in later figures is shown, which indicates the power-law exponents of the layer and the surrounding matrix.

adjacent synform) and the initial width of the modelling box, $\lambda_0/2$, is equal to half of the dominant wavelength, λ_d, which is a function of h_0, $\eta_{0,L}$, $\eta_{0,M}$, n_L, and n_M (Fletcher, 1974). However, for clarity reasons one entire wavelength is visualized in later figures (from the axial plane trace of one synform to the next). To avoid boundary effects, the lower and upper boundaries of the modelling box are set outside the zone of contact strain (Table 1). To generalize the results, all physical model parameters are non-dimensionalized using three characteristic values (Table 1).

3. Neutral line calculation and strain quantification

The FE model used to study the neutral lines in a progressively folding layer is described in Appendix A. Each FE simulation provides, among others, the velocity gradient tensor, $\dot{\mathbf{H}}$ with components $\dot{H}_{ij} = \partial v_i/\partial x_j$, at every integration point in the modelling domain and for every time step of the simulation. The strain rate tensor, $\dot{\boldsymbol{\varepsilon}}$, is calculated as $\dot{\boldsymbol{\varepsilon}} = (\dot{\mathbf{H}} + \dot{\mathbf{H}}^{\mathrm{T}})/2$, where the superscript T denotes the transpose of tensor $\dot{\mathbf{H}}$. The deformation gradient tensor, $\mathbf{F}$ (Haupt, 2002), at a given time step, m, is calculated from the velocity gradient tensor and the deformation gradient tensor of the preceding time step using the Euler integration method:

$$\mathbf{F}_m = \mathbf{F}_{m-1}\left[\mathbf{I} + \Delta t\dot{\mathbf{H}}_m\right] \tag{4}$$

where $\mathbf{I}$ is the identity matrix and Δt is the time increment. The deformation gradient tensor maps any vector from its initial undeformed state to its finite deformed state after time step m. For quantifying the finite strain the left Cauchy–Green tensor, $\mathbf{B}$ (Haupt, 2002), is used:

$$\mathbf{B} = \mathbf{F}\mathbf{F}^{\mathrm{T}} \tag{5}$$

All of these tensors are defined in the x_1–x_2-coordinate system. However, for calculating the neutral lines in the folding layer, the relevant quantities are the layer-parallel (i.e., tangential) strain rate and the layer-parallel finite strain. A standard tensor rotation (Ramsay and Huber, 1983) transforms the tensors from the global x_1–x_2-coordinate system to the local (i.e., different for every integration point) coordinate system consisting of the layer-parallel and the layer-perpendicular directions. At a given integration point of the layer the rotation angle is calculated as the weighted average of the two dip-angles at the closest points on the lower and upper interface of the folding layer. Using the rotated tensors two neutral lines can be defined.

(1) The incremental neutral line (INL) is the zero-contour line of the layer-parallel strain rate. It separates areas of incremental layer-parallel shortening from areas of incremental layer-parallel extension.
(2) The finite neutral line (FNL) is the zero-contour line of the finite layer-parallel strain. It separates areas of finite layer-parallel shortening from areas of finite layer-parallel extension.

The definitions of both neutral lines are different than the original definition of Ramsay (1967), i.e., the zero-contour line of the principal strain rates (INL) and of the principal finite strain (FNL). However, in a mechanically calculated symmetrical buckle fold with finite viscosity ratio between the layer and the surrounding matrix, the only place where these values can be zero is the axial plane trace. Therefore, Ramsay's definition of the neutral lines itself prevents the existence of the neutral lines, and only a finite and incremental neutral point on the axial plane trace can exist. Ramsay's definition can be applied in kinematical fold analysis using the idealized TLS strain pattern, but in mechanical models the definition given above has to be used. On the axial plane trace, the two definitions coincide.

For visualizing the finite strain in the numerical simulation snapshots, finite strain ellipses are plotted (Frehner and Schmalholz, 2006). They are calculated from the deformation gradient tensor. The two principal axes of a finite strain ellipse are given by the eigenvectors (direction) and the square roots of the eigenvalues (length) of the left Cauchy–Green tensor. In the following figures, two different measures for the background shortening are used. First and more intuitive, the shortening (i.e., negative elongation) is used:

$$e = (\lambda_d - \lambda)/\lambda_d \tag{6}$$

where λ is the current wavelength of the fold. Second, Schmalholz (2006) showed that for a Newtonian rheology the amplification history of a single-layer fold can be generalized, even up to high amplitudes, using the so-called scaled stretch,

$$S_S = \frac{\lambda_d}{\lambda}\left(\pi\sqrt{2\alpha_0}\frac{A_0}{\lambda_d}\right)^{\frac{1}{2+\alpha_0}} \tag{7}$$

Table 1
Model parameters used for numerical FE simulations.

Property	Symbol	Normalized value
Reference dynamic viscosity of matrix	$\eta_{0,M}$	Characteristic value
Initial thickness of layer	h_0	Characteristic value
Applied external strain rate	$\dot{\varepsilon}_{ext}$	Characteristic value
Reference dynamic viscosity of layer	$\eta_{0,L}/\eta_{0,M}$	[5,10,15,20,30,40,50, 70,100,150,200]
Power-law exponent of matrix	n_M	[1,3,5]
Power-law exponent of layer	n_L	[1,3,5]
Initial amplitude of layer	A_0/h_0	[0.001,0.1]
Dominant wavelength (=initial wavelength, $\lambda_0 = 2\times$ initial model width)	λ_d/h_0	$fct(\eta_{0,L}, \eta_{0,M}, n_L, n_M)$ (Fletcher 1974)
Constant C (Fig. 3)	C/h_0	15

where α_0 is the dimensionless initial growth rate of the fold calculated using the thick-plate formula of (Fletcher, 1977). Therefore, the scaled stretch is used for the Newtonian cases as the second measure for the background shortening.

4. Results

4.1. Newtonian single-layer folds

The simulation snapshots of a single-layer fold experiment using a Newtonian rheology, a viscosity ratio of 100 between the layer and the surrounding matrix, and an initial amplitude-to-thickness ratio of 0.1 is shown in Fig. 4. The fold hinge is of special importance, because this is the most common location for inner-arc-shortening structures or outer-arc-extension structures in natural folds. Therefore, Fig. 4 (upper-left diagram) also shows the positions of both neutral lines together with the layer-parallel strain rate evolution on the axial plane trace. The INL develops at a shortening of about 7% ($S_S \approx 1$) and first encloses only a small area at the outer arc with termination points at the outer interface of the layer. It migrates through the layer from the outer towards the inner arc with increasing shortening. On the axial plane trace, this migration is fast at the beginning (e.g., 45% through the layer after $e \approx 20\%$), slows down when the INL is close to the middle of the layer, and accelerates again towards the end of the simulation. The FNL develops after the INL at a shortening of about 15% ($S_S \approx 1.1$). It generally migrates slower than the INL from the outer towards the inner arc and stays behind the INL during the entire folding history. Therefore, there are always areas between the two neutral lines that exhibit a finite layer-parallel shortening but already experience an incremental layer-parallel extension. The fraction of the axial plane trace between the two neutral lines increases with increasing shortening and reaches around 50% of the total thickness of the layer towards the end of the simulation. With increasing shortening and fold amplification the termination points of the neutral lines switch from the outer to the inner interface of the layer. This happens at a shortening of about 31% ($S_S \approx 1.35$) for the INL and much later for the FNL at a shortening of about 70% ($S_S \approx 3.1$). In the late stages of the folding process both neutral lines enclose a small area at the inner arc. Even though this area of layer-parallel shortening becomes very small, it does not fully disappear up to the studied shortening of 74% ($S_S \approx 3.6$). It is important to notice that both neutral lines are discontinuous along the fold except for the instant, when the termination points switch from the outer to the inner interface.

Similar numerical simulations to the one presented in Fig. 4 were conducted, but with different viscosity ratios between the folding layer and the surrounding matrix (Table 1). Fig. 5 shows the positions of the neutral lines on the axial plane trace with increasing shortening (Fig. 5a) and scaled stretch (Fig. 5b) for these simulations. Because the scaled stretch depends on the material parameters (Eq. (7)), it is different for every simulation. For viscosity ratios larger than 40, the migration of the neutral lines is similar, except that the neutral lines appear later for smaller viscosity ratios (Fig. 5a). Plotted versus the scaled stretch (Fig. 5b), the migration curves of the INLs collapse on almost one single curve, particularly from the first appearance ($S_S \approx 1$) up to a scaled stretch of about 1.4. For decreasing viscosity ratios, the migration distance of the FNL from the outer arc into the layer decreases. Accordingly, the fraction of the axial plane trace that exhibits a finite layer-parallel shortening and an incremental layer-parallel extension increases with decreasing viscosity ratio. For

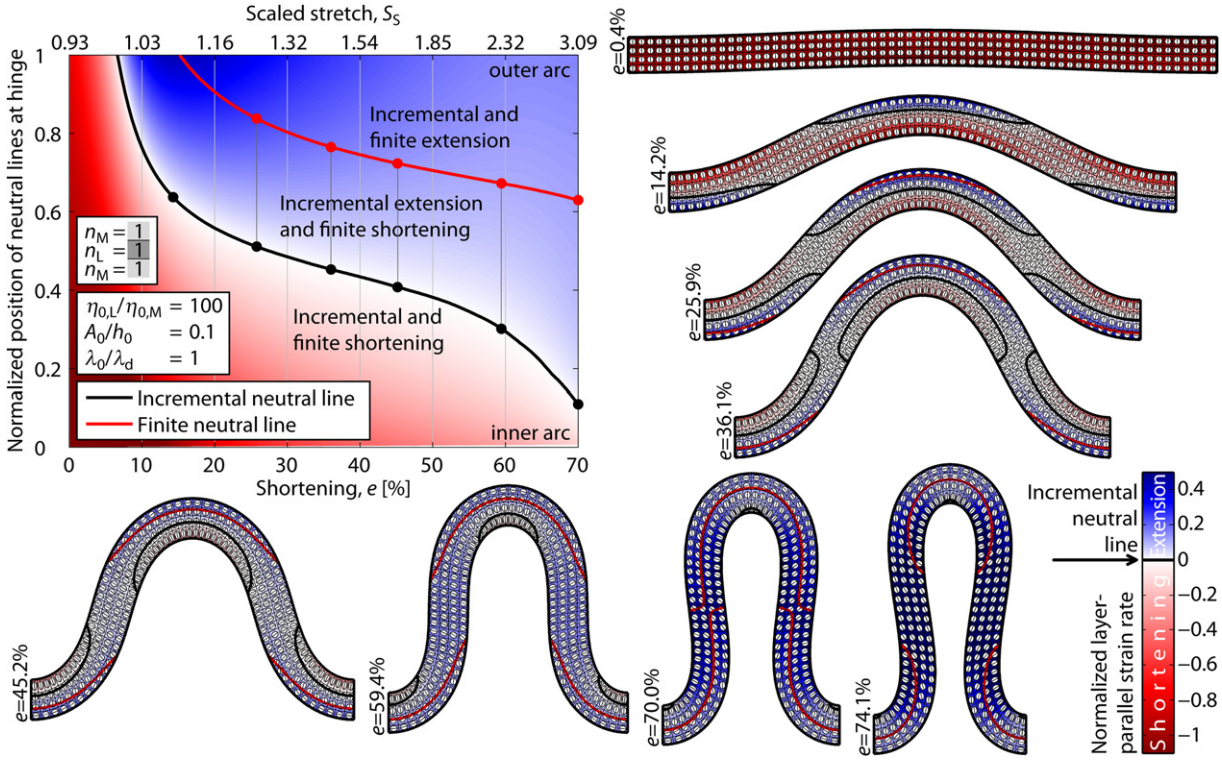

Fig. 4. Simulation snapshots of a progressively shortened Newtonian single-layer fold with the indicated modelling parameters. Colours represent the layer-parallel strain rate normalized by the absolute value of the externally applied strain rate, $\dot{\varepsilon}_{ext}$. The INL is drawn as a thick black line. The FNL is drawn as a thick red line. Finite strain ellipses with their major axis and a passive, initially orthogonal marker-grid are plotted. The upper-left diagram shows the layer-parallel strain rate and the positions of the two neutral lines on the axial plane trace, normalized by the current thickness of the layer at the hinge, with increasing shortening (and scaled stretch). The dots indicate the shortening for which the different simulation snapshots are plotted (For interpretation of the references to colour in this figure legend, the reader is referred to the web version of this article.)

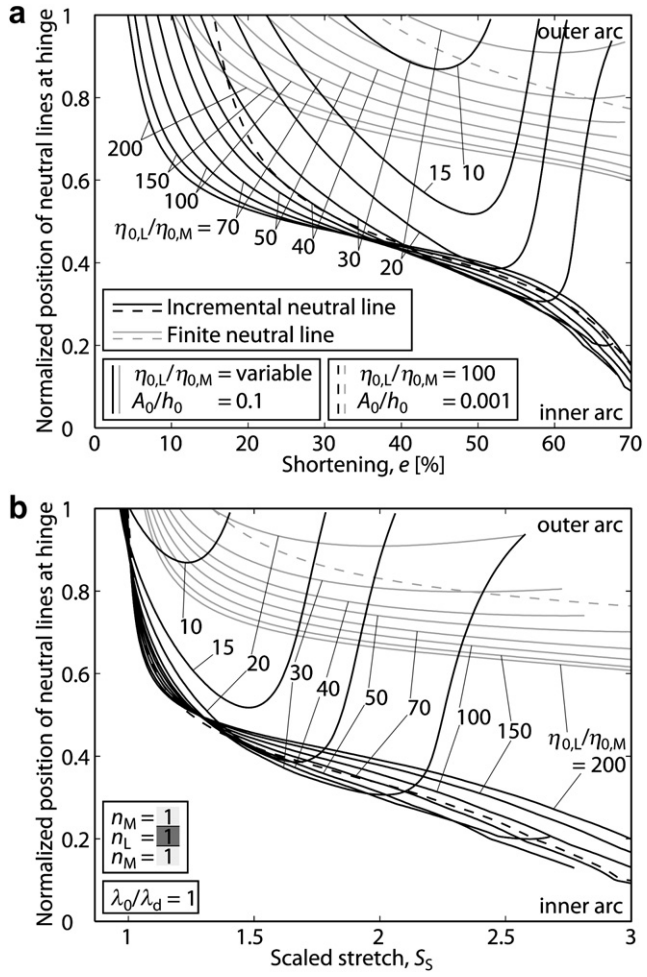

Fig. 5. Positions of the two neutral lines on the axial plane trace of a Newtonian single-layer fold, normalized by the current thickness of the layer at the hinge, with increasing shortening (a) and scaled stretch (b). The legend in (a) and the modelling parameters in (b) are valid for both subfigures.

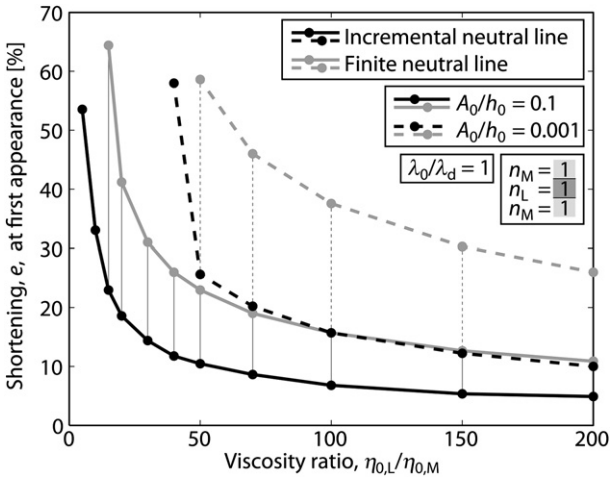

Fig. 6. Shortening value at the first appearance of the neutral lines in the single-layer fold for all simulations using a Newtonian rheology.

comparison, the neutral line migration curves of a simulation with a much smaller initial amplitude ($A_0/h_0 = 0.001$) and a viscosity ratio of 100 are shown in Fig. 5 as dashed lines. The neutral lines appear at a significantly larger shortening compared to the simulation with the same viscosity ratio but with larger initial amplitude. However, in Fig. 5b the INL collapses onto the same, almost unique curve as all other simulations with a viscosity ratio larger than 40.

For viscosity ratios smaller than 40 the neutral line migration at the fold hinge is different than described above for viscosity ratios larger than 40. The major difference is the INL, whose migration from the outer towards the inner arc eventually changes direction. The migration direction inverts at a shortening of about 59% ($S_S \approx 2.1$) for a viscosity ratio of 30 down to a shortening of about 44% ($S_S \approx 1.3$) for a viscosity ratio of 10. Despite this inversion, the INL first appears at a scaled stretch of about 1 (Fig. 5b), as for higher viscosity ratios. From Fig. 6, which shows the shortening at the first appearance of the neutral lines for all simulations using a Newtonian rheology, it is evident that both neutral lines appear later for decreasing viscosity ratio and for decreasing initial amplitude. This is in accordance with the observation of Ramberg (1964) that both a decreasing viscosity ratio and a decreasing initial amplitude lead to more layer-parallel shortening prior to buckling initiation. For an initial amplitude-to-thickness ratio of 0.1 and viscosity ratios lower than 15, no FNL develops up to the maximal studied shortening of 70% and the layer stays under finite layer-parallel shortening throughout the entire folding simulation. The same is true for an initial amplitude-to-thickness ratio of 0.001 and viscosity ratios lower than 50. For viscosity ratios lower than 40, even the INL does not develop. In this case, the fold amplification is so small that the layer-parallel shortening strain rate always exceeds the potential outer-arc extension.

4.2. Power-law viscous single-layer folds

A series of single-layer folding simulations have been performed with a power-law viscous behaviour in either the layer or both the layer and the surrounding matrix. The simulations exhibit a reference viscosity ratio of either 20 or 100. For a reference viscosity ratio of 100 (Fig. 7a), the migration of the INL at the fold hinge is similar for all simulations and, between 15% and 60% shortening, the INL-migration curves collapse on almost one single curve. The INL in the Newtonian case appears significantly later ($e \approx 7\%$) than in all power-law cases ($e < 3\%$). For a shortening larger than 60% a Newtonian matrix leads to an accelerated migration of the INL when the INL migrates away from the middle of the layer, while for a power-law viscous matrix the migration does not accelerate towards the end of the simulations. The migration of the FNL is similar for all power-law simulations, but significantly different than the Newtonian case, for which the FNL appears later than for all power-law cases.

The neutral line migration curves at the fold hinge for a reference viscosity ratio of 20 (Fig. 7b) are very different for the different simulations using a power-law viscous rheology. The neutral line migration curves do not collapse on an almost unique curve as for a reference viscosity ratio of 100. Common to all cases of a reference viscosity ratio of 20 is an inversion of the migration direction of the INL. Independently of the power-law exponent of the matrix, this inversion happens later for a power-law exponent of the layer of 3 compared to 5. For a visual comparison, Fig. 8 shows simulation snapshots of the simulations used to produce Fig. 7 at a shortening of 30% and 60%. Note that the dominant wavelength, and therefore the initial width of the model, is a function of the power-law exponent of both the layer and the matrix (Fletcher, 1974) and is different for each simulation (indicated in Fig. 8). For a reference viscosity ratio of 100, the fold geometries and the neutral line migration curves (Fig. 7) are similar for the simulations using

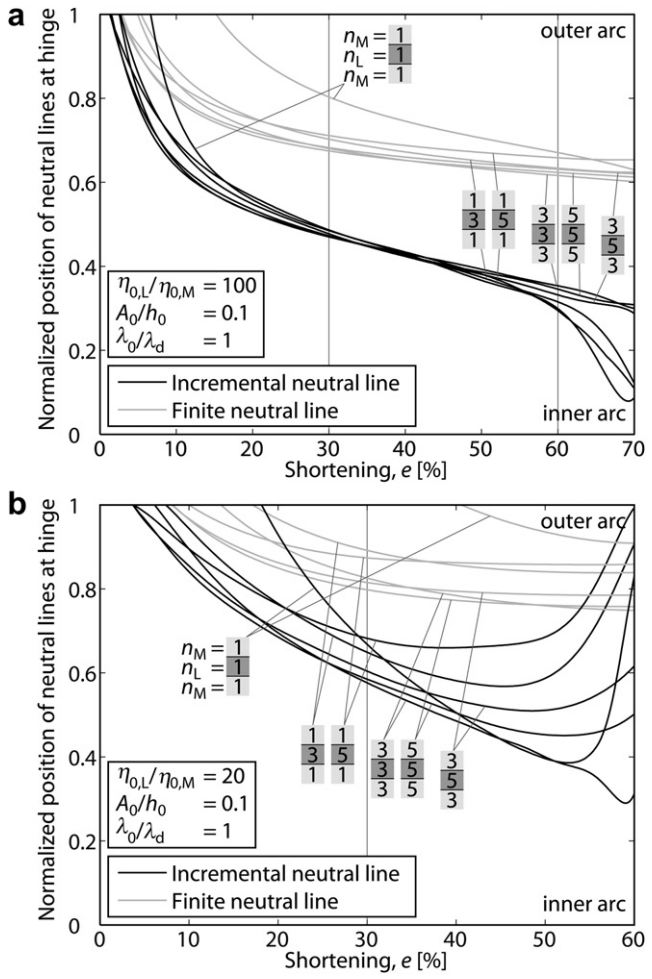

Fig. 7. Positions of the two neutral lines on the axial plane trace of different power-law single-layer folding simulations, normalized by the current thickness of the layer at the hinge, with increasing shortening. The reference viscosity ratio between the layer and the surrounding matrix is 100 (a) or 20 (b). The vertical lines indicate the shortening values used in Fig. 8.

different power-law exponents. For a reference viscosity ratio of 20 the fold geometry and the neutral line geometries are more complex than for a reference viscosity ratio of 100 and they can be very different for different applied power-law exponents. For example, at a late stage in the folding history (e.g., $e = 60\%$, right column in Fig. 8), multiple INL can develop along the axial plane trace. For these cases the INL already migrates towards the outer arc of the fold (Fig. 7). For a Newtonian matrix and a power-law exponent in the layer of 3, the INL is closer to the outer arc than the FNL. The area between the two neutral lines exhibits finite layer-parallel extension and incremental layer-parallel shortening. If the power-law exponent in the layer is increased to a value of 5, the INL already reached the outer arc at a background shortening of 60%. In this case, almost the entire axial plane trace experiences incremental layer-parallel shortening.

5. Discussion

The presented study shows that in a folding layer two neutral lines have to be distinguished, the incremental neutral line and the finite neutral line. Their dynamical behaviour and their positions in the layer are different from each other. For natural fold-related structures, such as outer-arc-extension structures or inner-arc-shortening structures, both of these neutral lines are relevant. For example, a common outer-arc-extension structure is a set of layer-perpendicular extensional fractures (Fig. 2). Such fractures open if the layer-parallel stress is tensile and exceeds the tensile strength of the folding layer. In the ideal case of a viscous layer the instantaneous deviatoric stress is proportional to the strain rate (Eq. (1)), but the total stress is also influenced by the pressure (overburden, pore-fluid pressure). Therefore, whether an extensional outer-arc fracture opens and how deep into the layer it penetrates may be related, but is not directly proportional to the position of the INL. The same applies to the inner-arc thrust (Fig. 1), whose initialization also depends on the instantaneous stress state. After their initialization, the progressive growth of such fold-related structures (i.e., amount of opening of extensional outer-arc fractures or net slip of inner-arc thrust) may be attributed to the cumulative strain, and therefore to the FNL, but a direct proportionality is also unlikely. Another common fold-related structure is the development of a foliation in the hinge area. The foliation can be perpendicular to the layer in the inner arc or parallel to the layer in the outer arc (Ramsay, 1967; Ramsay and Huber, 1987). In both cases the foliation is commonly assumed to reflect the finite strain state. Therefore, fold-related foliation may be attributed to the FNL.

In the presented numerical experiments, the neutral lines have only been considered in homogeneous isotropic layers, and the development of inner-arc-shortening structures and outer-arc-extension structures has not been modelled explicitly. However, the state of stress, strain and strain rate within the layer can be modified by these structures. For example, the opening of extensional outer-arc fractures modifies the stress state (Jäger et al., 2008) and therefore also modifies the state of strain and strain rate, or the development of a fold-related foliation introduces anisotropy in the layer and therefore changes the dynamical folding behaviour (Kocher et al., 2006). Such effects influence both the INL and the FNL, which in turn influence the further development of fold-related structures. This feedback mechanism has to be further investigated to fully understand the complex dynamical behaviour of the neutral lines in real rocks. However, already for the simple case of homogeneous isotropic layers, the presented study provides a mechanics-based insight into some of the complexities of the neutral lines.

Common to all different versions of TLS for the kinematical fold analysis (Bobillo-Ares et al., 2000, 2004, 2006; Bastida et al., 2003; Toimil and Fernandez, 2007; Lisle et al., 2009; Aller et al., 2010) is the assumption of a neutral line that is continuous along the fold. However, the presented FE simulations show that in a mechanical model of buckle folds none of the two neutral lines is continuous along the fold. Indeed (Toimil and Griera, 2007) showed that numerically modelled fold geometries cannot be kinematically reproduced by TLS alone. Usually, additional kinematical models, such as flexural flow or homogeneous pure-shear strain, are applied in sequence to TLS (e.g., in the FoldModeler-software; Bobillo-Ares et al., 2004) for a complete kinematical analysis of folds. As a result, the final kinematically constructed folds do not exhibit a continuous neutral line anymore (Bastida et al., 2003). While layer-parallel shortening prior to buckling initiation is an important mechanism (Ramberg, 1964) in both nature and the FE simulations, Hudleston et al. (1996) showed that flexural flow is an unlikely strain pattern in natural single-layer folds. TLS alone is a valid approximation of the strain pattern in folds with a large viscosity ratio to the surrounding matrix if the fold is close to parallel. The advantage of the kinematical fold analysis is the simplicity of the calculation rules to quantify and visualize the strain pattern and to calculate the shortening accumulated in natural folds. However, in addition to the kinematical study, the mechanical understanding of natural folds should be targeted. Mechanical and kinematical modelling approaches may improve

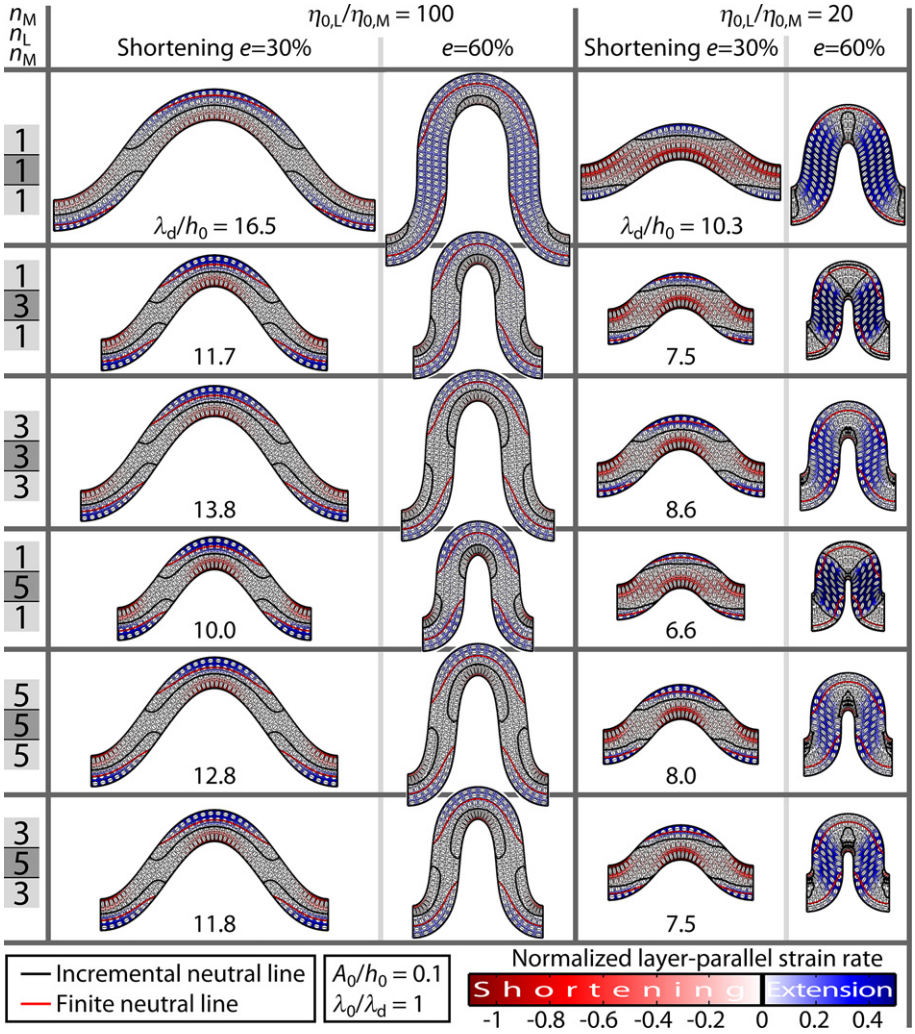

Fig. 8. Simulation snapshots of different power-law single-layer folding simulations after a shortening of 30% and 60%. The reference viscosity ratio between the layer and the surrounding matrix is 20 (two right columns) or 100. Colours represent the layer-parallel strain rate normalized by the absolute value of the externally applied strain rate, $\dot{\varepsilon}_{ext}$. The INL is drawn as a thick black line. The FNL is drawn as a thick red line. Finite strain ellipses with their major axis and a passive, initially orthogonal marker-grid are plotted. The dominant wavelength is indicated for each simulation. (For interpretation of the references to colour in this figure legend, the reader is referred to the web version of this article.)

one another, which will lead to better tools for reconstructing and mechanical and rheological understanding of natural folds.

In nature, folds are three-, rather than two-dimensional. Consequently, the description of neutral lines is not sufficient, but neutral surfaces have to be defined. However, many natural folds are close to cylindrical. In this case the neutral surfaces are also cylindrical and can be described by the neutral lines. For the more general case of non-cylindrical folds, the neutral surface can assume complex three-dimensional shapes. However, the investigation of such complex shapes was not the focus of the presented study and remains to be done in the future. Also, the presented study is limited to symmetrical folds with dominant initial wavelength. But this is a relevant geometry, because natural folds can sometimes be approximated as symmetrical folds, in particular in the hinge region. However, the dynamical behaviour of the neutral lines in asymmetrical and more irregular folds will be of great interest, but also remains to be done in the future.

6. Conclusions

From numerical FE simulations of the dynamical growth of single-layer buckle folds two neutral lines can be calculated and visualized: the incremental neutral line and the finite neutral line. The former is the zero-contour line of the layer-parallel strain rate; the latter is the zero-contour line of the finite layer-parallel strain. After their initialization at the outer arc of the fold hinge, both neutral lines migrate continuously towards the inner arc, whereas the INL migrates ahead of the FNL. For decreasing viscosity ratio between the folding layer and the surrounding matrix and decreasing initial amplitude, the neutral lines develop later during the folding process and, in some cases, no FNL or even none of the neutral lines develop and no extension occurs in the outer-arc. Both neutral lines are not continuous along the fold, but terminate either at the top or bottom interface of the folding layer. This contradicts the fundamental assumption of a continuous neutral line of the TLS strain pattern for kinematical fold analysis. For high reference viscosity ratios between the layer and the surrounding matrix (e.g., 100), the dynamical behaviour of the neutral lines in Newtonian and power-law viscous folds is similar. For small viscosity ratios (e.g., 20), the neutral lines in power-law viscous folds are substantially different for different power-law exponents, and different than the Newtonian case. In nature, fold-related structures can develop, such as inner-arc-shortening structures (e.g., enhanced foliation, thrusts) or outer-arc-extension structures (e.g., extensional fractures). Their development may depend on the position and the dynamical behaviour of one or both neutral lines in the fold.

Acknowledgements

This work was supported by the University of Vienna. The detailed and constructive reviews of Marcin Dabrowski and Fernando Bastida helped to improve this manuscript. Stefan M. Schmalholz is acknowledged for constructive inputs. Fernando O. Marques and Jean-Pierre Burg organized the field trip to Almograve, where intense discussions with Ulrike Exner, Jacqueline E. Reber, and Sarah M. Lechmann motivated this work.

Appendix A

An FE model has been self-developed (implementation in MATLAB) that solves the 2D plane-strain continuum mechanics equations for slowly deforming (i.e., no inertia terms) materials in the absence of gravity. The Newtonian version of the code is described in detail in Frehner and Schmalholz (2006). Both the power-law and the Newtonian version of the code are successfully benchmarked versus the analytical thick-plate folding solution of Fletcher (1974) and Fletcher (1977), respectively. Quickly summarized, the numerical implementation comprises a Lagrangian numerical grid consisting of isoparametric quadrilateral Q9/3-elements (Zienkiewicz and Taylor, 2000), a mixed velocity-pressure-penalty formulation of the governing equations using a Galerkin-approach (Hughes, 1987), and an Uzawa iteration (Pelletier et al., 1989) to enforce incompressibility. Different element integration schemes have been tested, and it was found that for the obtained distortion of the elements, a numerical integration on nine Gauss–Legendre quadrature points (Bathe, 1996) is sufficient. A higher number of quadrature points does not improve the results significantly. For the power-law version of the code, a Picard-iteration is implemented to converge to the correct solution (Schmalholz et al., 2008).

Supplementary material

An animated version of Figure 4 can be found as supplementary material in the online version of this article at doi:10.1016/j.jsg.2011.07.005.

References

Aller, J., Bobillo-Ares, N.C., Bastida, F., Lisle, R.J., Menendez, C.O., 2010. Kinematic analysis of asymmetric folds in competent layers using mathematical modelling. Journal of Structural Geology 32, 1170–1184. doi:10.1016/j.jsg.2010.07.008.

Bastida, F., Bobillo-Ares, N.C., Aller, J., Toimil, N.C., 2003. Analysis of folding by superposition of strain patterns. Journal of Structural Geology 25, 1121–1139.

Bastida, F., Aller, J., Bobillo-Ares, N.C., Toimil, N.C., 2005. Fold geometry: a basis for their kinematical analysis. Earth-Science Reviews 70, 129–164. doi:10.1016/j.earscirev.2004.11.006.

Bastida, F., Aller, J., Toimil, N.C., Lisle, R.J., 2007. Some considerations on the kinematics of chevron folds. Journal of Structural Geology 29, 1185–1200. doi:10.1016/j.jsg.2007.03.010.

Bathe, K.-J., 1996. Finite Element Procedures. Prentice Hall, Englewood Cliffs, ISBN 0-13-301458-4.

Bobillo-Ares, N.C., Bastida, F., Aller, J., 2000. On tangential longitudinal strain folding. Tectonophysics 319, 53–68.

Bobillo-Ares, N.C., Toimil, N.C., Aller, J., Bastida, F., 2004. FoldModeler: a tool for the geometrical and kinematical analysis of folds. Computers and Geosciences 30, 147–159. doi:10.1016/j.cageo.2003.09.008.

Bobillo-Ares, N.C., Aller, J., Bastida, F., Lisle, R.J., Toimil, N.C., 2006. The problem of area change in tangential longitudinal strain folding. Journal of Structural Geology 28, 1835–1848. doi:10.1016/j.jsg.2006.07.004.

Currie, J.B., Patnode, H.W., Trump, R.P., 1962. Development of folds in sedimentary strata. Geological Society of America Bulletin 73, 655–673.

Dieterich, J.H., 1969. Origin of cleavage in folded rocks. American Journal of Science 267, 155–165.

Dieterich, J.H., Carter, N.L., 1969. Stress-history of folding. American Journal of Science 267, 129–154.

Fletcher, R.C., 1974. Wavelength selection in the folding of a single layer with power-law rheology. American Journal of Science 274, 1029–1043.

Fletcher, R.C., 1977. Folding of a single viscous layer: exact infinitesimal-amplitude solution. Tectonophysics 39, 593–606.

Fossen, H., 2010. Structural Geology. Cambridge University Press, Cambridge, ISBN 978-0-521-51664-8.

Frehner, M., Schmalholz, S.M., 2006. Numerical simulations of parasitic folding in multilayers. Journal of Structural Geology 28, 1647–1657. doi:10.1016/j.jsg.2006.05.008.

Gairola, V.K., 1978. Strain distribution across an experimental single-layer fold. Tectonophysics 44, 27–40.

Haupt, P., 2002. Continuum Mechanics and Theory of Materials. Springer, Berlin, ISBN 3-540-43111-X.

Hudleston, P.J., Holst, T.B., 1984. Strain analysis and fold shape in a limestone layer and implications for layer rheology. Tectonophysics 106, 321–347.

Hudleston, P.J., Lan, L., 1993. Information from fold shapes. Journal of Structural Geology 15, 253–264.

Hudleston, P.J., Lan, L., 1995. Rheological information from geological structures. Pure and Applied Geophysics 145, 605–620.

Hudleston, P.J., Treagus, S.H., 2010. Information from folds: a review. Journal of Structural Geology 32, 2042–2071. doi:10.1016/j.jsg.2010.08.011.

Hudleston, P.J., Treagus, S.H., Lan, L., 1996. Flexural flow folding: does it occur in nature? Geology 24, 203–206.

Hughes, T.J.R., 1987. The Finite Element Method: Linear Static and Dynamic Finite Element Analysis. Dover Publications, Mineola, ISBN 0-4864-1181-8.

Jäger, P., Schmalholz, S.M., Schmid, D.W., Kuhl, E., 2008. Brittle fracture during folding of rocks: a finite element study. Philosophical Magazine 88, 3245–3263. doi:10.1080/14786430802320101.

Kocher, T., Schmalholz, S.M., Mancktelow, N.S., 2006. Impact of mechanical anisotropy and power-law rheology on single layer folding. Tectonophysics 421, 71–87. doi:10.1016/j.tecto.2006.04.014.

Lan, L., Hudleston, P.J., 1995. The effects of rheology on the strain distribution in single layer buckle folds. Journal of Structural Geology 17, 727–738.

Lechmann, S.M., Schmalholz, S.M., Burg, J.-P., Marques, F.O., 2010. Dynamic unfolding of multilayers: 2D numerical approach and application to turbidites in SW Portugal. Tectonophysics 494, 64–74. doi:10.1016/j.tecto.2010.08.009.

Lisle, R.J., Aller, J., Bastida, F., Bobillo-Ares, N.C., Toimil, N.C., 2009. Volumetric strains in neutral surface folding. Terra Nova 21, 14–20. doi:10.1111/j.1365-3121.2008.00846.x.

Pelletier, D., Fortin, A., Camarero, R., 1989. Are FEM solutions of incompressible flows really incompressible? (or how simple flows can cause headaches!). International Journal for Numerical Methods in Fluids 9, 99–112.

Price, N.J., Cosgrove, J.W., 1990. Analysis of Geological Structures. Cambridge University Press, Cambridge, ISBN 0-521-26581-9.

Ramberg, H., 1964. Selective buckling of composite layers with contrasted rheological properties, a theory for simultaneous formation of several orders of folds. Tectonophysics 1, 307–341.

Ramsay, J.G., 1967. Folding and Fracturing of Rocks. McGraw-Hill Book Company, New York. 07-051170-5.

Ramsay, J.G., Huber, M.I., 1983. The techniques of modern structural geology. In: Strain Analysis, vol. 1. Academic Press, London, ISBN 0-12-576921-0.

Ramsay, J.G., Huber, M.I., 1987. The techniques of modern structural geology. In: Folds and Fractures, vol. 2. Academic Press, London, ISBN 0-12-576922-9.

Schmalholz, S.M., 2006. Scaled amplification equation: a key to the folding history of buckled viscous single-layers. Tectonophysics 419, 41–53. doi:10.1016/j.tecto.2006.03.008.

Schmalholz, S.M., Schmid, D.W., Fletcher, R.C., 2008. Evolution of pinch-and-swell structures in a power-law layer. Journal of Structural Geology 30, 649–663. doi:10.1016/j.jsg.2008.01.002.

Shimamoto, T., Hara, I., 1976. Geometry and strain distribution of single-layer folds. Tectonophysics 30, 1–34.

Toimil, N.C., Fernandez, F.J., 2007. Kinematic analysis of symmetrical natural folds developed in competent layers. Journal of Structural Geology 29, 467–480. doi:10.1016/j.jsg.2006.10.001.

Toimil, N.C., Griera, A., 2007. Influence of viscosity contrast and anisotropy on strain accommodation in competent layers. Journal of Structural Geology 29, 787–801. doi:10.1016/j.jsg.2006.12.001.

Twiss, R.J., Moores, E.M., 2007. Structural Geology. W.H. Freeman and Company, New York, ISBN 0-7167-4951-3.

Zienkiewicz, O.C., Taylor, R.L., 2000. The finite element method. In: The Basis, vol. 1. Butterworth-Heinemann, Oxford, ISBN 0-7506-5049-4.